RESEARCH ARTICLE

Exploiting Hyperspectral Imaging and Optimal Deep Learning for Crop Type Detection and Classification

MASOUD ALAJMI[1], (Member, IEEE), **HANAN ABDULLAH MENGASH**[2],
MAJDY M. ELTAHIR[3], **MOHAMMED ASSIRI**[4], **SARA SAADELDEEN IBRAHIM**[5],
AND AHMED S. SALAMA[6]

[1]Department of Computer Engineering, College of Computers and Information Technology, Taif University, Taif 21944, Saudi Arabia
[2]Department of Information Systems, College of Computer and Information Sciences, Princess Nourah bint Abdulrahman University, Riyadh 11671, Saudi Arabia
[3]Department of Information Systems, College of Science and Art at Mahayil, King Khalid University, Abha 62529, Saudi Arabia
[4]Department of Computer Science, College of Sciences and Humanities-Aflaj, Prince Sattam bin Abdulaziz University, Al-Kharj 16273, Saudi Arabia
[5]Department of Computer and Self Development, Preparatory Year Deanship, Prince Sattam bin Abdulaziz University, Al-Kharj 16273, Saudi Arabia
[6]Department of Electrical Engineering, Faculty of Engineering and Technology, Future University in Egypt, New Cairo 11845, Egypt

Corresponding authors: Mohammed Assiri (m.assiri@psau.edu.sa) and Ahmed S. Salama (a.salama@fue.edu.eg)

ABSTRACT Hyperspectral imaging (HSI) plays a major role in agricultural remote sensing applications. Its data unit is the hyperspectral cube that contains spatial data in 2D but spectral band data of all the pixels in 3D. The classification accuracy of HSI was significantly enhanced by deploying either spatial or spectral features. HSIs are developed as a significant approach to achieve growth data monitoring and distinguish crop classes for precision agriculture, based on the reasonable spectral response to the crop features. The latest developments in deep learning (DL) and computer vision (CV) approaches permit the effectual detection and classification of distinct crop varieties on HSIs. At the same time, the hyperparameter tuning process plays a vital role in accomplishing effectual classification performance. The study introduces a dandelion optimizer with deep transfer learning-based crop type detection and classification (DODTL-CTDC) technique on HSI. The DODTL-CTDC technique makes use of the Xception model for the extraction of features from the HSI. In addition, the hyperparameter selection of the Xception model takes place using the DO algorithm. Moreover, the convolutional autoencoder (CAE) model is applied for the classification of crops into distinct classes. Furthermore, an arithmetic optimization algorithm (AOA) can be employed for optimal hyperparameter selection of the CAE model. The performance analysis of the DODTL-CTDC technique is assessed on the benchmark data set. The experimental outcomes demonstrate the betterment of the DODTL-CTDC method in the crop classification process.

INDEX TERMS Hyperspectral imaging, convolutional neural network, crop classification, agriculture, parameter tuning.

I. INTRODUCTION

Hyperspectral imaging (HSI) has received more importance in recent times [1]. Particularly, HSI classification has been an important source for real-world applications in domains

The associate editor coordinating the review of this manuscript and approving it for publication was Mu-Yen Chen.

namely mineral mapping, agriculture, environment, forestry, and so on. RS technology increases by leaps and bounds, the timeliness and resolution of RSIs are enhanced, and hyperspectral RS data are extensively utilized [2]. In particular, hyperspectral data perform an excellent part in agricultural surveys and are employed for monitoring crop conditions, estimating agricultural yield, monitoring pests,

etc. In agricultural surveys, fine classification of the HSI offers information on crop distribution [3]. Fine classification of crops needs images with high spectral as well as spatial resolution. Lately, airborne hyperspectral technology has grown quickly, and the applications of airborne HSI solve the aforementioned requirement. Several studies have been made on analyzing and employing HSI in the agriculture domain [4]. Reliable data about developing crops with various climatic conditions and agricultural resources and with distinct time stamps are highly significant and beneficial for agricultural expansion [5]. Improved RS technologies comprising HSI can fill the gap with outcomes namely crop classification and offer an appropriate performance [6].

Crop classification in RSI images is an important application in agriculture and land-use monitoring. It identifies and recognizes various kinds of crops or vegetation in satellite or aerial images. This information can be valuable for various purposes, including crop monitoring, yield estimation, land-use planning, and precision agriculture. The classical crop classification approaches depend on machine learning (ML) such as support vector machine (SVM), random forest (RF), and k-nearest neighbor (KNN) [7]. The classification method was difficult, the classification accuracy was usually lower, and the difficult spatial and temporal data of high-resolution RSIs have not been efficiently used. The ML subclasses of artificial intelligence (AI), and deep learning (DL) have a new domain of ML research. DL utilizes a multilayer ANN for performing several tasks, containing natural language processing (NLP) and computer vision (CV). This is a robust representation-learning method. The DL acquires multi-level feature representations utilizing non-linear modules. When compared to conventional SVM, RFs, and other techniques, abstract and deep features could be extracted [8]. Recently, several researchers have used DL methods for high-resolution and hyperspectral RSI classification tasks. Mono-temporal RSI classification depends on convolution neural network (CNN) and time series classification depends on recurrent neural network (RNN) are recently common techniques. CNN is a class of deep neural networks (DNN) [9], which can be particularly utilized for processing 2D shape modifications and has made breakthroughs in speech, video, audio, and image processing. Due to their capability for automatically identifying contextual features in image classification, CNN is commonly used to target identification and semantic segmentation tasks of high-resolution images [10].

This study presents a dandelion optimizer with a deep transfer learning-based crop type detection and classification (DODTL-CTDC) technique on HSI. The DODTL-CTDC technique makes use of the Xception model for the extraction of features from the HSI. In addition, the hyperparameter selection of the Xception model takes place using the DO algorithm. Moreover, the convolutional autoencoder (CAE) model is applied for the classification of crops into distinct classes. Furthermore, an arithmetic optimization algorithm (AOA) can be employed for optimal hyperparameter selection of the CAE model. The design of the DO and AOA

models for hyperparameter tuning demonstrates the novelty of the work. The performance analysis of the DODTL-CTDC method is tested on a benchmark dataset.

II. RELATED WORKS

A squirrel search optimization with a deep TL-aided crop classification (SSODTL-CC) approach on HSI was coined by Hamza et al. [11]. The developed method mainly designs a MobileNet with Adam optimizer to extract features. Additionally, the SSO technique with the BiLSTM approach was used for crop type classification. Alahmari et al. [12] developed a new HMAODL-CTC technique for crop-type classification methods on HSIs. This technique mostly aims to classify various types of crops on HSI. Further, this approach predominantly performs image pre-processing to enhance image quality. Moreover, the introduced method designs dilated CNN for extracting features. The HMAO method is employed for hyperparameter tuning. In [13], the authors target crop mapping for agriculture. Primarily, bands are divided based on their wavelength limits in near-infrared, shortwave infrared, and visible areas.

Xie et al. [14] emphasise techniques depending upon semantic segmentation and developed a novel transformer-based algorithm (HyperSFormer) to classify crops. The comprehensive approach adopts an easier and constant transformer design. Furthermore, the hyperpatch embedding (HPE) algorithm is utilized for extracting local spatial and spectral data from the HSI. The transpose padding upsamples (TPU) method was suggested for the model performance. Wei et al. [15] recommended an accurate crop classification approach utilizing spectral-spatial location fusion that depends on the conditional random field (SSLF-CRF) for UAV-borne hyperspectral RSI. The authors in [16] introduced a kernel tensor slice sparse coding-based classifier (KTSSCC) for crop classification of UAV H2 images. The kernel tensor depiction model in KTSSCC will decrease the non-linear distinction while maintaining the spectral as well as spatial features of land cover.

In [17], the GLCM texture, morphological profiles and end member abundance features are exploited using the spatial data of the HSI. Later, the number of spatial data is combined with the spectral information for making classification outcomes by employing DNN with CRF (DNN+CRF) technique. The CRF regards both contextual and spatial data for minimizing misclassification noises. Li et al. [18] analysed and compared a crop classification application that depends on DL techniques and various time-series information to use the probability of enhancing the accuracy of crop classification. Time series classification databases are built depending on spectral stacking and vegetation indexes (VIs) using multi-temporal Sentinel-2 images.

III. THE PROPOSED DODTL-CTDC MODEL

In this study, we have introduced an automatic crop recognition model by the use of DL named DODTL-CTDC technique on HSI. The goal of the presented model is to
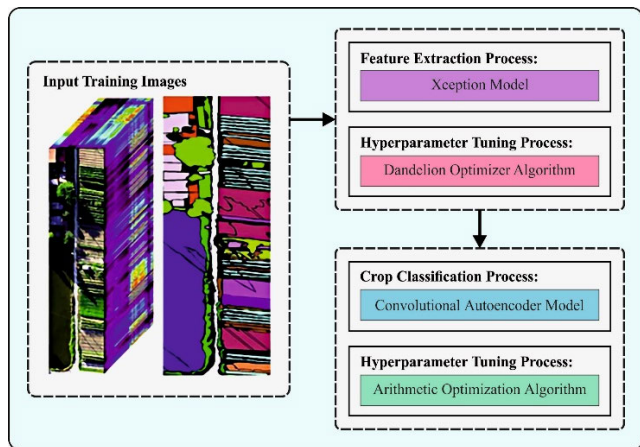
FIGURE 1. The overall flow of DODTL-CTDC methodology.

accomplish automated and accurate crop classification on HSI. The DODTL-CTDC technique comprises four stages of operations Xception feature extraction, DO-based hyperparameter tuning, CAE classification, and AOA-based hyperparameter optimization. Fig. 1 describes the entire process of the DODTL-CTDC method.

A. OPTIMAL FEATURE EXTRACTION

In this work, the Xception method was executed for the extracting of feature vectors. During the DODTL-CTDC method, the Xception architecture has been harnessed for feature extraction in hyperspectral images. Xception is a DL approach that is generally designed for CV tasks, specifically image classification. Specific convolution layers like depthwise separable convolutional are employed in the Xception design to capture significant spectral data. These layers perform spectral filters, discerning intricate patterns and features from the hyperspectral data, so enabling the model to efficiently extract spectral signatures connected with several crop types. By leveraging the power of the Xception model, the DODTL-CTDC methodology makes sure that meaningful spectral features are extracted for precise crop classification from the hyperspectral image.

The feature extraction of the baseline network consists of 36 convolution layers [19]. The Xception model is linearly stacked on residual connection depthwise convolution layer. Compared with Inception_v2 or Inception_v3, which are considerably highly difficult to define, this makes it quite easy to adapt and construct; using high-level frameworks including TensorFlow. Transfer learning (TL) is to train the Xception architecture. As said by Ian Goodfellow et al. TL is an ML approach where a model constructed for one work is transmitted to other corresponding activities, utilizing previous information from the task related to speed up the learning. In general, TL often takes place in DL since the model should be trained on challenging and large datasets that demand extensive resources. Francois Chollet presents a complete description of the Xception architecture. Every 14 units including the 36 Conv layers encompass linear

residual connection. First, the input flow (8 Conv layers and 4 modules) processes the data, then the middle flow (3 Conv layers and 1 module), and the exit flow (4 Conv layers and 2 modules).

The preparation and model design is explained in the following:

Binary-cross-entropy (log or logarithmic loss) is used to evaluate the prediction probability for the binary classification dataset based on Eq. (1) for Model Compilation. Xception architecture is the baseline model, where TL is used for training the last layer through image net weight.

$$LogLoss = -\left((1-y)*\log\left(1-\hat{y}\right) + y*\log\left(\hat{y}\right)\right) \quad (1)$$

In Eq. (1), y and $\hat{y}$ denotes the expected and the predicted values.

Here, the DO technique is exploited to fine-tune the hyperparameters of the Xception model such as learning rate, number of epochs, and batch size. DO is a bio-inspired optimization technique which mimics the proceeding of DO fight to different places based on the wind; this procedure is divided into three stages [20]. During the rising stage, the seed rises in a spiral fashion due to the influence of drag force; this can be attained during sunny weather. Moreover, in rainy climates, the dandelion seed diffuses within the local region. This alteration in rising provides two scenarios of searching, such as randomly settling in various locations due to the influences of wind as well as weather, eventually increasing into a new dandelion.

The DO algorithm depends on the iterative evolution of the early population like other metaheuristic approaches. D indicates the variable dimension, and P denotes the population size.

$$population = \begin{bmatrix} X_1^1 & \cdots & X_1^D \\ \vdots & \ddots & \vdots \\ X_P^1 & \cdots & X_P^D \end{bmatrix} \quad (2)$$

In terms of the optimization algorithm, every individual generated is signified as X_i and is subjected to the lower bound (LB) and upper bound (UB) of the problems.

$$X_i = rand \times (UB - LB) + LB \quad (3)$$

In Eq. (3), $rand$ is a random integer within [1, 2] and i refers to the integer range from 1 to P.

In the initialization process, consider the optimum fitness values as initial elite X_{elite}, as follows:

$$\begin{cases} X_{elite} = (find\,(f_{best} == f\,(X_i))) \\ f_{best} = \min\,(f\,(X_i)) \end{cases} \quad (4)$$

In Eq. (4), $find()$ denotes the two indexes with equivalent values.

In the rising stage, the behaviour of dandelion seeds was affected by the climate condition, with two potential instances. Dandelion seeds ascend to considerable height during clear weather conditions:

$$X_{t+1} = X_t + \alpha \times v_x \times v_y \times \ln Y \times (X_s - X_t) \quad (5)$$

In Eq. (5), X_t denotes the location of the dandelion seed at t iteration, α indicates the adaptive parameter for adjusting the search step length, X_s shows the random location, $\ln Y$ refers to the *log* uniform distribution subjected to $\mu = 0$ and $\sigma^2 = 1$, and 0_χ and 0_y denotes the lift component coefficient of the dandelion seed.

$$X_s = rand\,(1,D) \times (UB - LB) + LB \tag{6}$$

$$\ln Y = \begin{cases} \dfrac{1}{y\sqrt{2\pi}} exp\left(-\dfrac{1}{2\sigma^2}(\ln y)^2\right) & y \geq 0 \\ 0 & y < 0 \end{cases} \tag{7}$$

$$\alpha = rand\,() \times \left(\frac{1}{t_{\max}^2}t^2 - \frac{2}{t_{\max}}t + 1\right) \tag{8}$$

$$\begin{cases} v_x = r \times \cos\theta \\ v_y = r \times \sin\theta \\ r = \dfrac{1}{e^\theta} \end{cases} \tag{9}$$

From the expression, y denotes the uniform distribution [0, 1], t_{mox} indicates the maximal iteration count and θ shows the randomly generated value within $[-\pi, \pi]$.

During inclement weather, especially on rainy days, the DO seeds can't properly rise due to air resistance.

$$X_{t+1} = X_t \times k \tag{10}$$

In Eq. (10), k denotes the regulator of the local search range.

$$\begin{cases} q = \dfrac{1}{t_{\max}^2 - 2t_{\max} + 1}t^2 - \dfrac{2}{t_{\max}^2 - 2t_{\max} + 1} \\ \quad t + 1 + \dfrac{1}{t_{\max}^2 - 2t_{\max} + 1} \\ k = 1 - rand() \times q \end{cases} \tag{11}$$

During the descending stage, they steadily drop after the DO seeds rise to a specific altitude as follows:

$$X_{t+1} = X_t - \alpha \times \beta_t \times (X_{mean-t} - \alpha \times \beta_t \times X_t) \tag{12}$$

In Eq. (12), β_t denotes the Brownian movement and $X_{measn-t}$ shows the mean location of the population as follows:

$$X_{mean\_t} = \frac{1}{P}\sum_{i=1}^{P} X_i \tag{13}$$

In the seeds' descent, individual evolution can be defined by the mean location. Then, the dandelion seeds randomly select where they will land is named as landing stage:

$$X_{t+1} = X_{elite} + levy\,(\lambda) \times \alpha \times (X_{elite} - X_t \times \delta) \tag{14}$$

In Eq. (14), δ shows the linear increasing function between [1, 2], X_{elite} denotes the optimum location of the dandelion seeds, and $levy(\lambda)$ indicates the function of Levy fight. The DO algorithm designs a fitness function to attain improved classification performance. It determines a positive integer to represent the better performance of the candidate solutions. In this study, the minimization of the classification error rate is considered as the fitness function.

B. IMAGE CLASSIFICATION

For crop type classification, the CAE model is used. CAE is a specific kind of autoencoder (AE) that integrates the capability of CNNs to effectively extract image features and the capability of AE to represent the input dataset [21]. In the DODTL-CTDC approach, the CAE roles a vital play in crop classification. The CAE model contains convolutional and deconvolutional layers, with max-pooling and activation functions combined for dimensionality reduction and feature extraction. In the training, the CAE acquires for encoding hyperspectral data as a low-dimensional latent space while maintaining vital spectral data. The CAE reconstruction task, decreasing the difference between input and output, supports it to capture discriminative features from the hyperspectral data that are subsequently utilized for precise crop classification. The number of layers and their certain configuration can vary but are planned to efficiently distill spectral signatures that separate various crop types in the hyperspectral image.

AE regenerate the input by fusing two neural networks (NN) components: an encoder and a decoder. The encoder units encode the input x to hidden output l viz., compressed form of the input. The dimensionality of hidden output l is smaller than the dimensionality of input x. Then, the decoder relies on hidden output, l, and produces output $\tilde{x}$ to the input x. AE was trained to minimise the reconstructed loss of the network for reconstructing the original inputs. The AE comprises encoder $f(x, \theta)$ that compresses the data and decoder $g(l, \phi)$ that reconstructs the input can be mathematically modelled as follows.

$$l = f\,(x, \theta) \tag{15}$$

$$\tilde{x} = g\,(l, \phi) = g\,(f\,(x, \theta), \phi) \tag{16}$$

where θ and ϕ denote the trained parameter of the encoder and decoder, correspondingly. This parameter was set by training the AE to minimise the cost function.

$$\mathcal{C}\,(x, \tilde{x}) = \mathcal{L}\,(x, \tilde{x}) + regularization\,term \tag{17}$$

Now, $\mathcal{L}(x, \tilde{x})$ indicates a reconstructed loss function i.e., a binary cross-entropy (*BCE*) or mean squared error (*MSE*) averaged over the overall amount of samples which are evaluated as follows:

$$\mathcal{L}_{MSE} = \frac{1}{N}\sum_{i}^{N}\left(x^i - \tilde{x}^i\right)^2 \tag{18}$$

$$\mathcal{L}_{BCE} = \frac{1}{N}\sum_{i}^{N} -\left[x^i \log\left(\tilde{x}^i\right) + \left(1 - \tilde{x}^i\right)\log\left(1 - \tilde{x}^i\right)\right] \tag{19}$$

In Eq. (17), the regularization term is essential for DNN to prevent the network from learning identity function and thereby improve the generalization capability of the model. Shallow network AE needn't include regularization terms because the bottleneck architecture itself is adequate to enforce the regularization. In CAEs, the pooling layer prevents the over-fitting of the network and enhances the

generalization capability. Therefore, the reconstructed loss was used as a cost function. The encoder of CAE comprises an alternative layer of convolution and pooling for the FC and network layers. A hidden layer is signified as an FC layer (1D layer). The decoder mainly comprises of a sequence of transposed convolution layers with FC layers. A CAE includes three major operations such as upsampling, convolution, and pooling which are subsequently explained.

C. HYPERPARAMETER TUNING USING AOA

Finally, the AOA adjusts the parameters related to the CAE algorithm such as learning rate, batch size, kernel size, and number of layers. The fundamental AOA operation includes initialization, exploitation, and exploration [22]. Fig. 2 illustrates the flowchart of AOA.

(a) Initialization. The candidate solution (XA) was randomly generated. The existing population is signified as a matrix xa. DM represents the dimension. NP denotes the number of individuals y. The better solution is the optimal solution achieved for all the iterations.

$$XA = \begin{bmatrix} xa_{1,1} & \cdots & xa_{1,DM-1} & xa_{1,DM} \\ xa_{2,1} & \cdots & xa_{2,DM-1} & xa_{2,DM} \\ \vdots & \cdots & \vdots & \vdots \\ xa_{NP,1} & \cdots & xa_{NP,DM-1} & xa_{NP,DM} \end{bmatrix} \quad (20)$$

Using the math optimizer accelerated (MOA) function, the search phase was selected as an exploration or exploitation.

$$MOA(iter) = miniter + iter \times \left(\frac{maxiter - miniter}{Miter} \right) \quad (21)$$

In Eq. (21), $Miter$ refers to maximum iteration. $iter$ denotes the present round. $miniter$ and $maxiter$ are the minimum and maximum values of MOA, correspondingly. (b) Exploration. When $r_1 > MOA$, the Division or Multiplication operator is implemented, as follows:

$$xa_{i,j}(iter+1) = \begin{cases} best(xa_j) \div (MOP + \varepsilon) \times ((UB_j - LB_j) \\ \times \mu+, LB_j), \ r_2 > 0.5 \\ best(xa_j) \times MOP \times ((UB_j - LB_j) \\ \times \mu + LB_j) \ r_2 \leq 0.5 \end{cases} \quad (22)$$

where r_2 denotes a random integer. $best(xa_j)$ shows the jth location in the optimum solution. ε represents a small value.

The higher and lower boundaries of $the j^{th}$ location are represented as UB_j and $LB_j. \mu$ is fixed as 0.5.

$$MOP(iter) = 1 - \frac{iter^{\frac{1}{\alpha}}}{Miter^{\frac{1}{\alpha}}} \quad (23)$$

In Eq. (23), α shows the sensitive parameter set as 5.

TABLE 1. Description on dataset1.

Dataset-1	
Class	No. of Samples
Corn	1000
Cotton	1000
Sesame	1000
Broad-leaf soybean	1000
Narrow-leaf soybean	1000
Rice	1000
Water	1000
Roads and houses	1000
Mixed weed	1000
Total Samples	9000

(c) Exploitation. When $r_1 \leq MOA$, the Addition (A) or Subtraction (S) operators are implemented.

$$xa_{i,j}(iter+1) = \begin{cases} best(xa_j) - (MOP + \varepsilon) \times ((UB_j - LB_j) \\ \times \mu+, LB_j), \ r_3 > 0.5 \\ best(xa_j) + MOP \times ((UB_j - LB_j) \\ \times \mu + LB_j) \ r_3 \leq 0.5 \end{cases} \quad (24)$$

The present optimum fitness is compared with the prior optimum fitness, and the lower value determines the last optimum solution. Fitness selection is a key aspect of the AOA methodology. An encoder performance has been deployed to design the optimum result of candidate performance. At present, the accuracy value is the major form deployed to develop a fitness function.

$$Fitness = \max(P) \quad (25)$$

$$P = \frac{TP}{TP + FP} \quad (26)$$

w, FP and TP denote the false and true false positive values.

IV. RESULTS AND DISCUSSION

The experimental outcome of the DODTL-CTDC method was carried out against 2 databases [23], namely dataset1 (WHU-Hi-LongKou) and dataset2 (WHU-HiHanChuan). The dataset1 comprises a total of 9000 instances with nine classes containing 1000 instances under all the classes as shown in Table 1. Further, dataset-2 includes a total of 11,000 samples with 11 classes, holding 1000 instances under all the classes as represented in Table 2.

Fig. 3 shows the classifier analysis of the DODTL-CTDC approach on dataset1. Figs. 3a-3b represents the confusion matrix achieved by the DODTL-CTDC technique at 70:30 of the training (TR) set/testing (TS) set. Similarly, Fig. 3c reveals the PR curve and Fig. 3d depicts the ROC study of the DODTL-CTDC methodology.

In Table 3 and Fig. 4, brief crop classifier results of the DODTL-CTDC technique are reported on dataset1. The results identified that the DODTL-CTDC technique properly categorises all classes. With 70% of TR set,
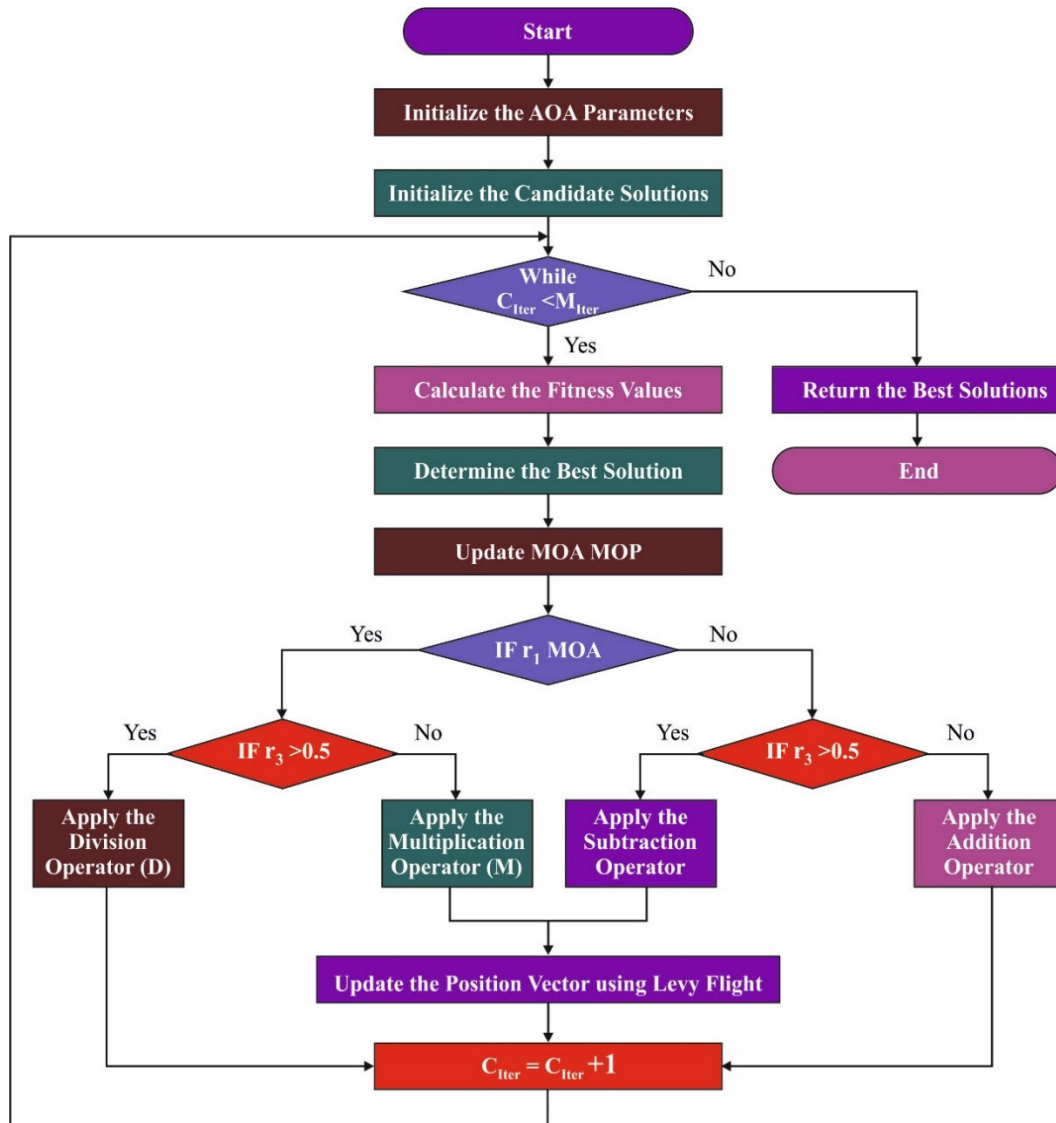
FIGURE 2. Flowchart of AOA.

the DODTL-CTDC technique offers an average $accu_y$ of 99.42%, $prec_n$ of 97.45%, $reca_l$ of 97.38%, and F_{score} of 97.39%. Besides, with 30% of TS set, the DODTL-CTDC approach offers an average $accu_y$ of 99.42%, $prec_n$ of 97.45%, $reca_l$ of 97.38%, and F_{score} of 97.39%.

Fig. 5 illustrates the training accuracy TR_accu_y and VL_accu_y of the DODTL-CTDC method on dataset1. The TL_accu_y is defined by the estimation of the DODTL-CTDC system on the TR dataset whereas the VL_accu_y is calculated by evaluating the performance on an individual testing dataset. The outcomes exhibited that TR_accu_y and VL_accu_y rise with an upsurge in epochs. Therefore, the performance of the DODTL-CTDC algorithm gets enhanced on the TR and TS dataset with an increase in several epochs.

In Fig. 6, the TR_loss and VR_loss analysis of the DODTL-CTDC method on dataset 1 is demonstrated. The TR_loss determines the error between the predicted performance and original values on the TR data. The

VR_loss signifies the measure of the performance of the DODTL-CTDC system on separate validation data. The outcomes indicated that the TR_loss and VR_loss tend to reduce with increasing epochs. It described the improved performance of the DODTL-CTDC algorithm and its ability to generate accurate classification. The decreased value of TR_loss and VR_loss shows the higher performance of the DODTL-CTDC approach in capturing relationships and patterns.

Fig. 7 shows the classifier analysis of the DODTL-CTDC method on dataset2. Figs. 7a-7b represents the confusion matrix attained by the DODTL-CTDC technique on 70:30 of the TR set/TS set. The simulation value signified that the DODTL-CTDC system has recognized and classified all 11 classes accurately. Similarly, Fig. 7c revealed the PR curve of the DODTL-CTDC technique. The figure reported that the DODTL-CTDC algorithm has obtained maximal PR performance on 11 class labels. Eventually,
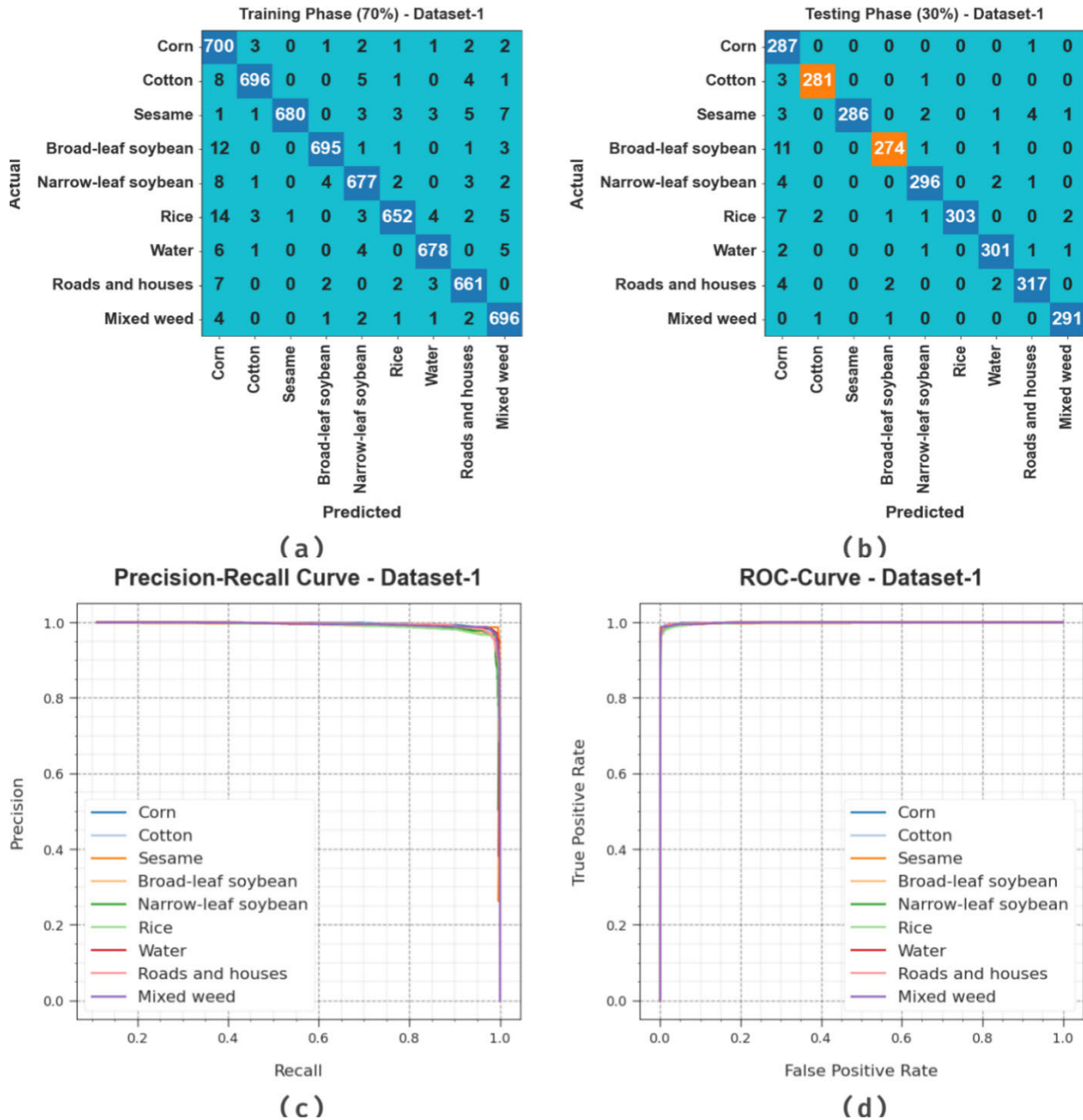
FIGURE 3. Performances on dataset1 (a-b) Confusion matrices, (c) PR_curve, and (d) ROC.

Fig. 7d demonstrates the ROC analysis of the DODTL-CTDC approach. The outcome value depicted that the DODTL-CTDC method has led to able solutions with superior ROC outcomes on 11 classes.

In Table 4 and Fig. 8, a comprehensive crop classification analysis of the DODTL-CTDC approach is reported on dataset2. The outcomes identified that the DODTL-CTDC method properly categorises all class labels. With 70% of TR set, the DODTL-CTDC system offers an average $accu_y$ of 97.66%, $prec_n$ of 87.20%, $reca_l$ of 87.15%, and F_{score} of 87.14%. Also, with 30% of TS set, the DODTL-CTDC algorithm offers an average $accu_y$ of 97.65%, $prec_n$ of 87.09%, $reca_l$ of 87.02%, and F_{score} of 87.02%.

Fig. 9 illustrates the training accuracy TR_accu_y and VL_accu_y of the DODTL-CTDC method on dataset2. The TL_accu_y is defined by the estimation of the DODTL-CTDC system on the TR dataset whereas the VL_accu_y is calculated by evaluating the performance on an individual testing dataset. The outcomes exhibited that TR_accu_y and VL_accu_y rise with an upsurge in epochs. Hence, the performance of the DODTL-CTDC approach gets enhanced on the TR and TS dataset with an increase in the number of epochs.

In Fig. 10, the TR_loss and VR_loss analysis of the DODTL-CTDC method on dataset2 is demonstrated. The TR_loss determined the error between the predictive performance and original values on the TR data. The VR_loss

TABLE 2. Description on dataset2.

Dataset-2	
Class	No. of Samples
Class1	1000
Class2	1000
Class3	1000
Class4	1000
Class5	1000
Class6	1000
Class7	1000
Class8	1000
Class9	1000
Class10	1000
Class11	1000
Total Samples	11000

TABLE 3. Crop classifier outcome of DODTL-CTDC approach on dataset1.

Dataset1				
Class	$Accu_y$	$Prec_n$	$Reca_l$	F_{Score}
Training Phase (70%)				
Corn	98.86	92.11	98.31	95.11
Cotton	99.56	98.72	97.34	98.03
Sesame	99.62	99.85	96.73	98.27
Broad-leaf soybean	99.59	98.86	97.48	98.16
Narrow-leaf soybean	99.37	97.13	97.13	97.13
Rice	99.32	98.34	95.32	96.81
Water	99.56	98.26	97.69	97.98
Roads and houses	99.48	97.21	97.93	97.56
Mixed weed	99.43	96.53	98.44	97.48
Average	99.42	97.45	97.38	97.39
Testing Phase (30%)				
Corn	98.70	89.41	99.65	94.25
Cotton	99.74	98.94	98.60	98.77
Sesame	99.59	100.00	96.30	98.11
Broad-leaf soybean	99.37	98.56	95.47	96.99
Narrow-leaf soybean	99.52	98.01	97.69	97.85
Rice	99.52	100.00	95.89	97.90
Water	99.59	98.05	98.37	98.21
Roads and houses	99.44	97.84	97.54	97.69
Mixed weed	99.78	98.64	99.32	98.98
Average	99.47	97.72	97.65	97.64

FIGURE 4. Average result of DODTL-CTDC approach on dataset1.

FIGURE 5. $Accu_y$ curve of DODTL-CTDC methodology on dataset1.

FIGURE 6. Loss curve of DODTL-CTDC methodology on dataset1.

signified the measure of the performance of the DODTL-CTDC system on separate validation data. The outcomes indicated that the *TR_loss* and *VR_loss* tend to minimize with increasing epochs. It depicted the improved performance of the DODTL-CTDC method and its ability to generate accurate classification. The decreased value of *TR_loss* and *VR_loss* exhibits the higher performance of the DODTL-CTDC algorithm in capturing relationships and patterns.
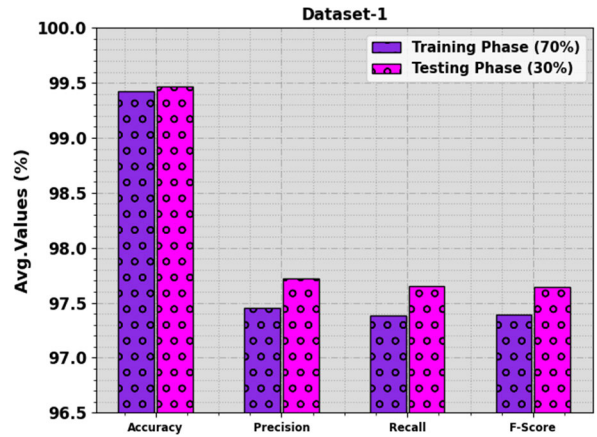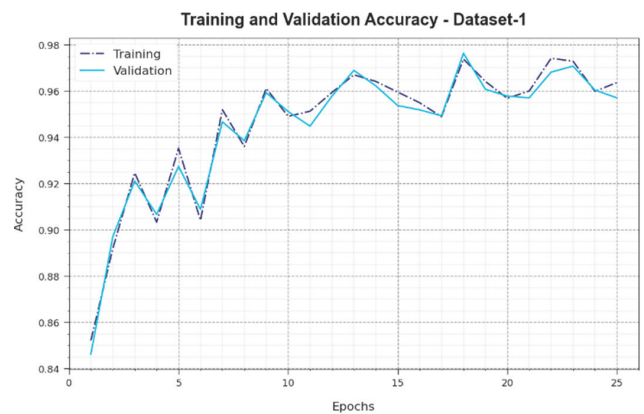
In Table 5, a widespread comparative investigation of the DODTL-CTDC technique is depicted on two datasets [11]. The results highlighted that the DODTL-CTDC technique accomplishes effectual performance on both datasets.

In Fig. 11, a brief comparison study of the DODTL-CTDC technique takes place on dataset1. The figure represented that the SVM model exhibits the least $accu_y$ of 95.98%. Along with that, the FNEA-OO, SVRFMC, CNN, and CNN-CRF approaches demonstrate slightly improved $accu_y$ values of
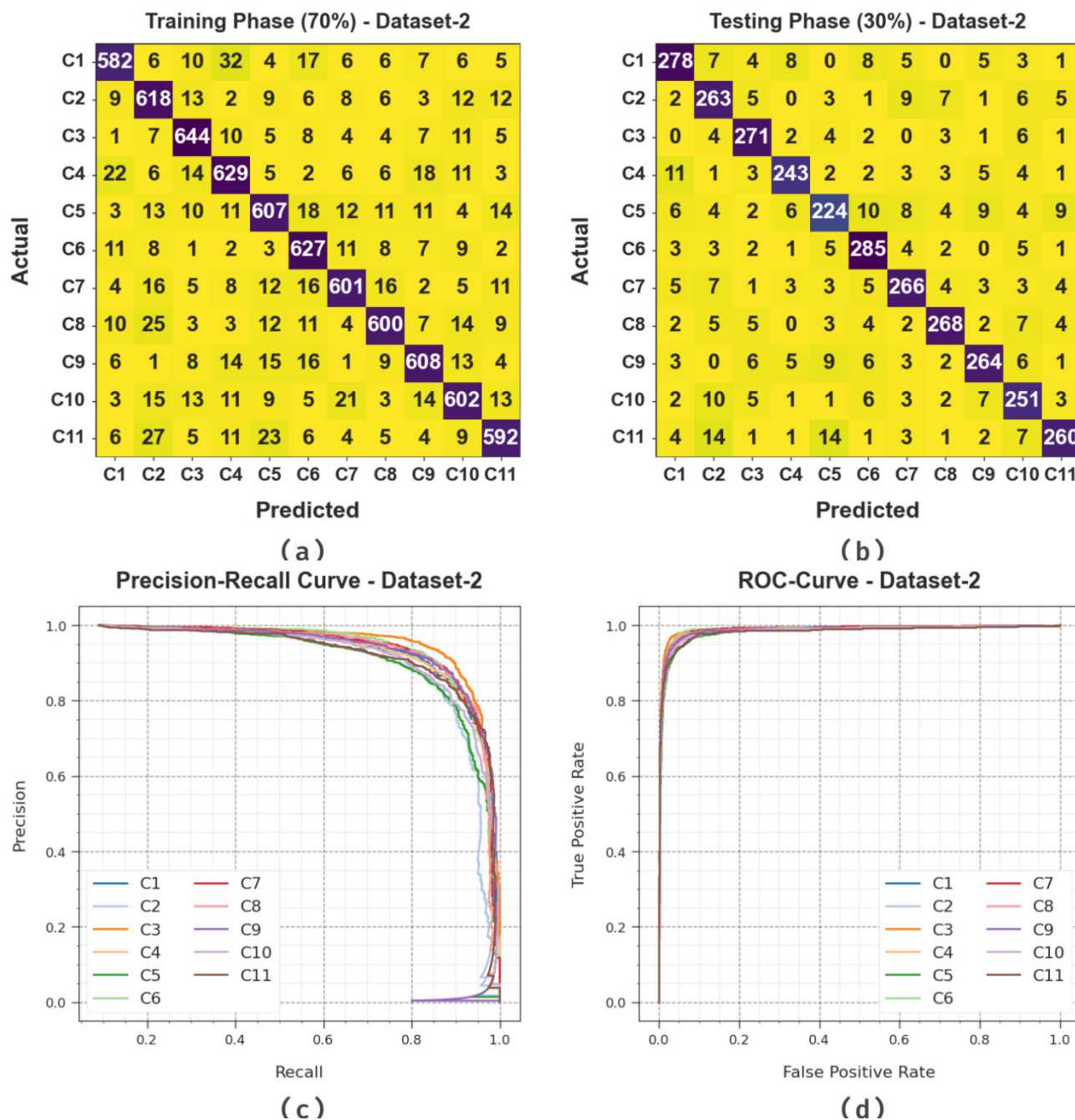
FIGURE 7. Performances on dataset2 (a–b) Confusion matrices, (c) PR_curve, and (d) ROC.

97.07%, 98.20%, 98.08%, and 98.80% correspondingly. Nevertheless, the DODTL-CTDC technique reported better results with a maximum $accu_y$ of 99.47%.

In Fig. 12, a detailed comparison analysis of the DODTL-CTDC method takes place on dataset2. The figure denoted that the SVM technique reveals the least $accu_y$ of 95.98%. Along with that, the FNEA-OO, SVRFMC, CNN, and CNN-CRF algorithms show slightly enhanced $accu_y$ values of 97.07%, 98.20%, 98.08%, and 98.80% correspondingly. While the SSODTL-CC technique demonstrates considerable outcome with $accu_y$ of 99.23%. However, the

DODTL-CTDC system reported better results with a greater $accu_y$ of 99.47%.

These outcomes highlighted the effective crop classification solution of the DODTL-CTDC methodology. The DODTL-CTDC approach reveals higher outcomes related to existing approaches because of their innovative combination of deep TL, hyperparameter optimizer utilizing the DO, and CAE for crop classification from the hyperspectral image. The combination of the Xception method, renowned for its feature extraction abilities, make sure the effectual extraction of relevant spectral data. Additionally, the employment

TABLE 4. Crop classifier result of DODTL-CTDC approach on dataset2.

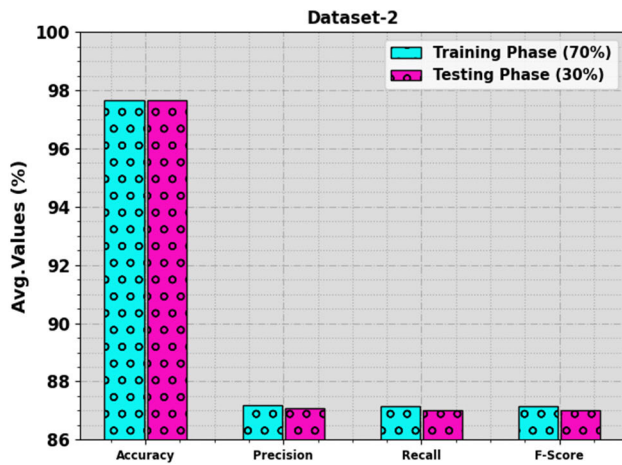| Dataset2				
Class	$Accu_y$	$Prec_n$	$Reca_l$	F_{Score}
Training Phase (70%)				
Class-1	97.74	88.58	85.46	87.00
Class-2	97.35	83.29	88.54	85.83
Class-3	98.13	88.71	91.22	89.94
Class-4	97.44	85.81	87.12	86.46
Class-5	97.35	86.22	85.01	85.61
Class-6	97.83	85.66	91.00	88.25
Class-7	97.77	88.64	86.35	87.48
Class-8	97.77	89.02	85.96	87.46
Class-9	97.83	88.37	87.48	87.92
Class-10	97.39	86.49	84.91	85.69
Class-11	97.69	88.36	85.55	86.93
Average	97.66	87.20	87.15	87.14
Testing Phase (30%)				
Class-1	97.61	87.97	87.15	87.56
Class-2	97.15	82.70	87.09	84.84
Class-3	98.27	88.85	92.18	90.48
Class-4	98.12	90.00	87.41	88.69
Class-5	96.79	83.58	78.32	80.87
Class-6	97.85	86.36	91.64	88.92
Class-7	97.64	86.93	87.50	87.21
Class-8	98.12	90.54	88.74	89.63
Class-9	97.70	88.29	86.56	87.42
Class-10	97.24	83.11	86.25	84.65
Class-11	97.64	89.66	84.42	86.96
Average	97.65	87.09	87.02	87.02

FIGURE 8. Average outcome of DODTL-CTDC approach on dataset2.

TABLE 5. $Accu_y$ outcome of DODTL-CTDC algorithm with other methods on two databases [11].

Methods	Dataset1	Dataset2
SVM Model	95.98	77.34
FNEA-OO	97.07	86.49
SVRFMC	98.20	86.95
CNN Algorithm	98.08	87.72
CNN-CRF	98.80	94.67
SSODTL-CC	99.23	97.15
DODTL-CTDC	99.47	97.66

of the DO improves hyperparameter tuning precision, contributing to optimized model efficiency. The incorporation of the CAE technique for crop classification provides a strong

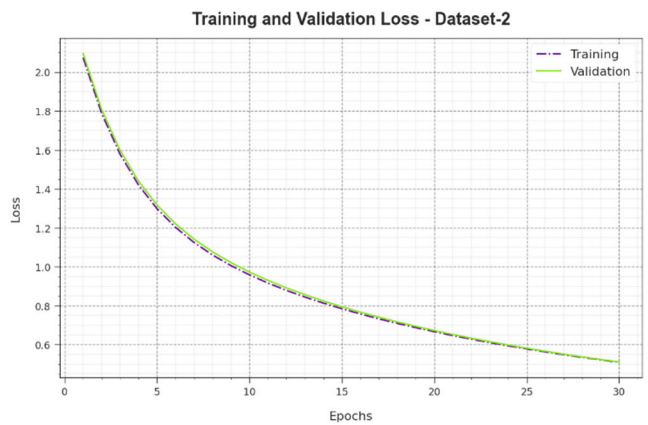**FIGURE 9.** $Accu_y$ curve of DODTL-CTDC approach on dataset2.

FIGURE 10. Loss curve of DODTL-CTDC approach on dataset2.
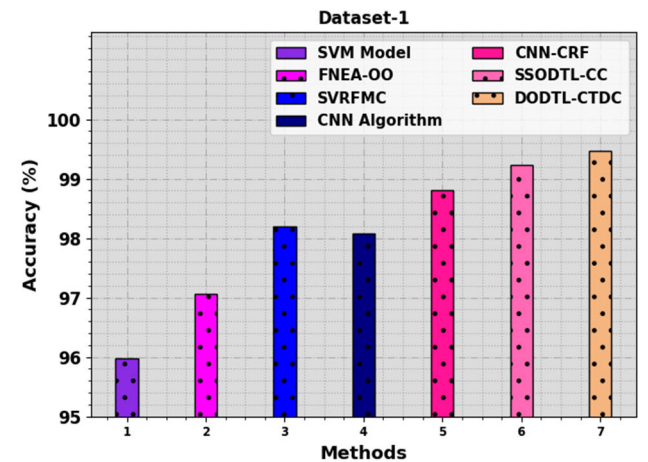

FIGURE 11. $Accu_y$ outcome of DODTL-CTDC algorithm on dataset1.

framework for distinguishing crop varieties correctly. This holistic method outcomes in better classification accuracy, making the DODTL-CTDC methodology a vital advancement in the field of agricultural remote sensing and hyperspectral image analysis.
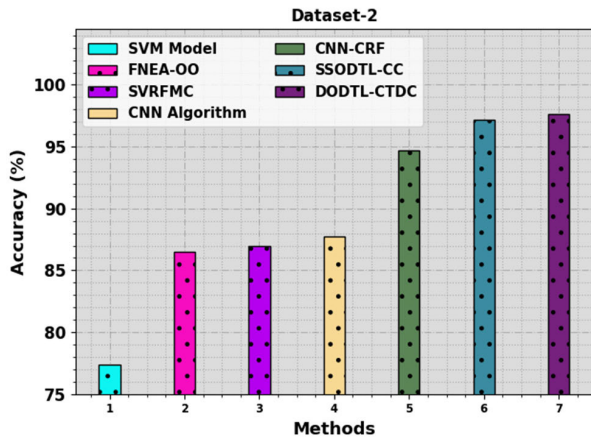
FIGURE 12. *Accu$_y$* outcome of DODTL-CTDC algorithm on dataset2.

V. CONCLUSION

In this study, we have introduced an automated crop classification model using DL named DODTL-CTDC technique on HSI. The goal of the presented model is to accomplish automated and accurate crop classification on HSI. The DODTL-CTDC technique comprises four stages of operations Xception feature extraction, DO-based hyperparameter tuning, CAE classification, and AOA-based hyperparameter optimization. In this work, the hyperparameter selection of the Xception model takes place using the DO algorithm. Finally, the AOA can be employed for optimal hyperparameter selection of the CAE algorithm. The performance analysis of the DODTL-CTDC technique is tested on a benchmark dataset. The experimental outcomes demonstrate the betterment of the DODTL-CTDC method in the crop classification process. In the future, the crop classification accuracy of the DODTL-CTDC technique can be improved by the feature fusion process.

REFERENCES

[1] K. Bhosle and V. Musande, "Evaluation of deep learning CNN model for land use land cover classification and crop identification using hyperspectral remote sensing images," *J. Indian Soc. Remote Sens.*, vol. 47, no. 11, pp. 1949–1958, Nov. 2019.

[2] K. Bhosle and B. Ahirwadkar, "Deep learning convolutional neural network (CNN) for cotton, mulberry and sugarcane classification using hyperspectral remote sensing data," *J. Integr. Sci. Technol.*, vol. 9, no. 2, pp. 70–74, 2021.

[3] U. Patel, M. Pathan, P. Kathiria, and V. Patel, "Crop type classification with hyperspectral images using deep learning : A transfer learning approach," *Model. Earth Syst. Environ.*, vol. 9, no. 2, pp. 1977–1987, Jun. 2023.

[4] Y. Zhang, D. Wang, and Q. Zhou, "Advances in crop fine classification based on hyperspectral remote sensing," in *Proc. 8th Int. Conf. Agro-Geoinformatics (Agro-Geoinformatics)*, Jul. 2019, pp. 1–6.

[5] H. Li, C. Zhang, Y. Zhang, S. Zhang, X. Ding, and P. M. Atkinson, "A scale sequence object-based convolutional neural network (SS-OCNN) for crop classification from fine spatial resolution remotely sensed imagery," *Int. J. Digit. Earth*, vol. 14, no. 11, pp. 1528–1546, Nov. 2021.

[6] M. A. Duhayyim, H. Alsolai, S. B. H. Hassine, J. S. Alzahrani, A. S. Salama, A. Motwakel, I. Yaseen, and A. S. Zamani, "Automated deep learning driven crop classification on hyperspectral remote sensing images," *Comput., Mater. Continua*, vol. 74, no. 2, pp. 3167–3181, 2023.

[7] P. Sadeghi-Tehran, N. Virlet, and M. J. Hawkesford, "A neural network method for classification of sunlit and shaded components of wheat canopies in the field using high-resolution hyperspectral imagery," *Remote Sens.*, vol. 13, no. 5, p. 898, Feb. 2021.

[8] L. Wei, M. Yu, Y. Zhong, J. Zhao, Y. Liang, and X. Hu, "Spatial–spectral fusion based on conditional random fields for the fine classification of crops in UAV-borne hyperspectral remote sensing imagery," *Remote Sens.*, vol. 11, no. 7, p. 780, Apr. 2019.

[9] V. M. Scholl, J. McGlinchy, T. Price-Broncucia, J. K. Balch, and M. B. Joseph, "Fusion neural networks for plant classification: Learning to combine RGB, hyperspectral, and LiDAR data," *PeerJ*, vol. 9, Jul. 2021, Art. no. e11790.

[10] N. Farmonov, K. Amankulova, J. Szatmári, A. Sharifi, D. Abbasi-Moghadam, S. M. M. Nejad, and L. Mucsi, "Crop type classification by DESIS hyperspectral imagery and machine learning algorithms," *IEEE J. Sel. Topics Appl. Earth Observ. Remote Sens.*, vol. 16, pp. 1576–1588, 2023.

[11] M. A. Hamza, F. Alrowais, J. S. Alzahrani, H. Mahgoub, N. M. Salem, and R. Marzouk, "Squirrel search optimization with deep transfer learning-enabled crop classification model on hyperspectral remote sensing imagery," *Appl. Sci.*, vol. 12, no. 11, p. 5650, Jun. 2022.

[12] S. Alahmari, S. Yonbawi, S. Racharla, E. L. Lydia, M. K. Ishak, H. K. Alkahtani, A. Aljarbouh, and S. M. Mostafa, "Hybrid multi-strategy Aquila optimization with deep learning driven crop type classification on hyperspectral images," *Comput. Syst. Sci. Eng.*, vol. 47, no. 1, pp. 375–391, 2023.

[13] L. Agilandeeswari, M. Prabukumar, V. Radhesyam, K. L. N. B. Phaneendra, and A. Farhan, "Crop classification for agricultural applications in hyperspectral remote sensing images," *Appl. Sci.*, vol. 12, no. 3, p. 1670, Feb. 2022.

[14] J. Xie, J. Hua, S. Chen, P. Wu, P. Gao, D. Sun, Z. Lyu, S. Lyu, X. Xue, and J. Lu, "HyperSFormer: A transformer-based end-to-end hyperspectral image classification method for crop classification," *Remote Sens.*, vol. 15, no. 14, p. 3491, Jul. 2023.

[15] L. Wei, M. Yu, Y. Liang, Z. Yuan, C. Huang, R. Li, and Y. Yu, "Precise crop classification using spectral–spatial-location fusion based on conditional random fields for UAV-borne hyperspectral remote sensing imagery," *Remote Sens.*, vol. 11, no. 17, p. 2011, Aug. 2019.

[16] L. Yang, J. Chen, R. Zhang, S. Yang, X. Zhang, and L. Jiao, "Precise crop classification of UAV hyperspectral imagery using kernel tensor slice sparse coding based classifier," *Neurocomputing*, vol. 551, Sep. 2023, Art. no. 126487.

[17] L. Wei, K. Wang, Q. Lu, Y. Liang, H. Li, Z. Wang, R. Wang, and L. Cao, "Crops fine classification in airborne hyperspectral imagery based on multi-feature fusion and deep learning," *Remote Sens.*, vol. 13, no. 15, p. 2917, Jul. 2021.

[18] Q. Li, J. Tian, and Q. Tian, "Deep learning application for crop classification via multi-temporal remote sensing images," *Agriculture*, vol. 13, no. 4, p. 906, Apr. 2023.

[19] M. Abubakr, M. Rady, K. Badran, and S. Y. Mahfouz, "Application of deep learning in damage classification of reinforced concrete bridges," *Ain Shams Eng. J.*, May 2023, Art. no. 102297.

[20] A. Elhammoudy, M. Elyaqouti, E. H. Arjdal, D. B. Hmamou, S. Lidaighbi, D. Saadaoui, I. Choulli, and I. Abazine, "Dandelion optimizer algorithm-based method for accurate photovoltaic model parameter identification," *Energy Convers. Manag., X*, vol. 19, Jul. 2023, Art. no. 100405.

[21] D. Arumugam and R. Kiran, "Compact representation and identification of important regions of metal microstructures using complex-step convolutional autoencoders," *Mater. Design*, vol. 223, Nov. 2022, Art. no. 111236.

[22] L. Peng, C. Sun, and W. Wu, "Effective arithmetic optimization algorithm with probabilistic search strategy for function optimization problems," *Data Sci. Manage.*, vol. 5, no. 4, pp. 163–174, Dec. 2022.

[23] Y. Zhong, X. Hu, C. Luo, X. Wang, J. Zhao, and L. Zhang, "WHU-hi: UAV-borne hyperspectral with high spatial resolution (H^2) benchmark datasets and classifier for precise crop identification based on deep convolutional neural network with CRF," *Remote Sens. Environ.*, vol. 250, Dec. 2020, Art. no. 112012.